Journal of Nuclear Materials 385 (2009) 346–350

Contents lists available at ScienceDirect

Journal of Nuclear Materials

journal homepage: www.elsevier.com/locate/jnucmat

Microprobe analysis of neutron irradiated and autoclaved zirconium niobium claddings using synchrotron-based hard X-ray imaging and spectroscopy

A. Froideval [a,*], S. Abolhassani [a], D. Gavillet [a], D. Grolimund [a,b], C. Borca [a,b], J. Krbanjevic [c], C. Degueldre [a]

[a] Paul Scherrer Institut, Nuclear Energy and Safety, 5232 Villigen PSI, Switzerland
[b] Paul Scherrer Institut, Swiss Light Source, 5232 Villigen PSI, Switzerland
[c] Ecole Polytechnique Fédérale de Lausanne, Centre de Recherches en Physique des Plasmas, Lausanne, Switzerland

ARTICLE INFO

PACS:
28.41.Qb
78.40.Kc
61.80.Hg
61.05.cj
68.37.Yz

ABSTRACT

Two zirconium alloys (Zr–2.5%Nb) – one oxidized in a pressurized water reactor, the other oxidized in autoclave and used as reference – are analyzed by combining synchrotron-based scanning transmission and fluorescence X-ray microscopy and micro-X-ray absorption spectroscopy (micro-XAS). Two-dimensional zirconium distribution maps recorded on the neutron irradiated and the non-irradiated autoclaved Zr–2.5%Nb alloys clearly allow the localization of the oxide and the metal parts of the interface with a micrometer spatial resolution. Micro-XAS investigations make possible the determination of the speciation of zirconium and niobium both in the oxide and the metal parts of the interface for the irradiated and non-irradiated samples. The coordination environment and/or the valency of zirconium and niobium in the metal and the oxide parts of the interface have been determined for both materials, and interpreted on the basis of comparison with metal and oxide reference compounds.

1. Introduction

Zirconium-based alloys are extensively used as materials for fuel claddings, pressure tubes in CANDU reactors and to a certain extent for other structural components such as fuel channels, in various types of operating nuclear reactors. The properties of zirconium alloys depend on the chemical composition and the heat treatment of the alloy for each type of reactor. It has been demonstrated by several studies that the variation of the chemical composition of the alloys such as the addition of niobium can considerably improve the corrosion resistance of the claddings materials [1–5]. The structure and composition of oxides formed on different zirconium alloys have been subject of several investigations in the past e.g. [6–13]. One of the requirements of the cladding being its resistance to corrosion, the aim of these examinations is to correlate the oxidation behaviour of the alloys to the structure and composition of the oxide layers formed at the surface of the alloys in different oxidation environments. The oxidation state, e.g. the oxidation state of different secondary phases present in the oxide layer, is one parameter which has been investigated. Certain precipitates (e.g. $Zr(Fe,V)_2$ Laves phases in Zr-based alloys) [9] have been observed to remain metallic in the oxide in the vicinity of the interface. Niobium containing alloys have also shown a similar behaviour. As an example, studies performed on autoclaved materials [10] as well as on irradiated materials [11] have revealed Nb-rich metallic phases in the vicinity of the metal–oxide interface in the oxide layer. The oxidation state of the niobium in autoclaved materials has been studied in detail in Zr–2.5%Nb as well as in Zr–20%Nb alloys by scanning electron microscopy (SEM) and transmission electron microscopy (TEM) [10]. These authors have demonstrated that the β-Nb and Nb-rich phases show a delayed oxidation and remain metallic in the vicinity of the metal–oxide interface in the zirconium oxide matrix. They ultimately oxidize to form an amorphous oxide. The same behaviour is observed for irradiated Zr–Nb alloys examined by TEM [11,14]. As the oxidation state of different atoms can be determined on an averaged scale by X-ray absorption spectroscopy (XAS), effort is made to use this technique to further examine the speciation of zirconium and niobium in Zr–Nb alloys. The present study concerns the spectroscopic investigations of a zirconium niobium alloy with a niobium concentration of 2.5 wt.%. The analysis of the formal valency and/or the coordination environment of zirconium and niobium both in the oxide and the metal sides of the metal–oxide interface for an irradiated and non-irradiated Zr–2.5%Nb alloys is performed by means of micro-XAS. The results are discussed and interpreted on the basis of comparison with spectroscopic data recorded on metal and oxide reference compounds.

* Corresponding author. Tel.: +41 56 310 44 48; fax: +41 56 310 35 65.
E-mail address: annick.froideval@psi.ch (A. Froideval).

0022-3115/$ - see front matter © 2008 Elsevier B.V. All rights reserved.
doi:10.1016/j.jnucmat.2008.12.022

2. Experimental

2.1. Description of materials

A Zr–2.5%Nb cladding segment of a fuel rod irradiated in a pressurized water reactor (PWR) and a non-irradiated Zr–2.5%Nb tube section oxidized in an autoclave have been used for this study.

The irradiated fuel rod was exposed for three reactor cycles at 600 K under a pressure of 15 MPa and had an average burn up of 41.4 MW d kg^{-1}. The neutron fluence of the segment studied has been estimated to be approximately of 8.3×10^{21} cm^{-2} ($E > 0.821$ MeV). The oxide thickness of the segment has been determined by scanning electron microscopy (SEM). The details of the microstructure of this neutron irradiated sample are already provided in [11]. Briefly, the material shows a Nb-rich phase which has precipitated in the form of platelets. The Nb-rich regions can be observed both in the metal and the oxide, and they show a delayed oxidation with respect to the zirconium matrix in the vicinity of the metal–oxide interface. The autoclaved Zr–2.5%Nb alloy used as reference material has been oxidized at 620 K under a pressure close to 10 MPa. This sample has also been analyzed by SEM in order to determine the thickness of its oxide layer. Additional compounds such as NbO, NbO_2 and Nb_2O_5 niobium oxides purchased from Alfa Aesar and Aldrich as well as a niobium metal sample have been used as reference materials in this study.

2.2. Sample preparation

Both the neutron irradiated and the autoclaved reference Zr–2.5%Nb materials have been prepared by focused ion beam (FIB). The used 'NVision 40' workstation from Carl Zeiss (Germany) is equipped with an electron column (GEMINI SEM) having a high resolution field emission gun and a zeta FIB system. This system allows high speed sputtering of the material for the early stages of sample preparation. The samples are milled and continuously imaged by SEM during preparation.

A small tube segment of 1 mm × 2 mm, is mounted on the holder, with the oxide layer perpendicular to the ion beam, in order to create a small thinned window for spectroscopic measurements. A window with 30 μm in axial, and 20 μm in circumferential orientations is milled using a gallium ion beam. The acceleration voltage for the sputtering has been of 30 kV and the beam current has been of 45 nA for fast sputtering and removal of material, and of 80 pA for final polishing. The final thickness of the small window cut in the irradiated sample is experimentally determined from the SEM image to be close to 10 μm. Both irradiated and non-irradiated autoclaved samples are prepared under similar conditions and geometry.

2.3. High resolution 2D images and X-ray absorption spectra

The microscopic and spectroscopic measurements conducted on the FIB manufactured Zr–2.5%Nb samples have been carried out at the micro XAS beam line of the Swiss Light Source (SLS, Villigen, Switzerland) [15]. This analytical facility is the unique SLS beam line allowing for the investigation of radioactive materials by means of high intensity hard X-ray synchrotron radiation with a micro-focused X-ray beam. In the present work, the micro XAS beamline has been set up in order to deliver monochromatic X-rays tuned to the photon energy of either Zr or Nb K-edge for elemental selectivity by means of a double crystal monochromator using a pair of Si (1 1 1) crystals. The final X-ray spot size at the sample surface is close to 1 μm × 1 μm. A specific specimen holder, on which the samples are mounted at 90° with respect to the incident photon beam to minimize the X-ray spot size at the sample surface, is positioned on a 3 axis-motion manipulator. This manipulator allows an accurate positioning of the sample with respect to the photon beam.

The element-resolved speciation of zirconium atoms in the irradiated and in the autoclaved Zr–2.5%Nb materials have been investigated using the following two-step measurement strategy: (i) two-dimensional ~40 μm × 50 μm high resolution scanning map recorded at 18.2 keV, i.e. above the Zr K-edge, in transmission detection mode with a micrometer spatial resolution; and (ii) absorption spectra recorded at the Zr K-edge using a micron-focused hard X-ray beam for two sample positions (one in the metal and one in the oxide parts of the interface). The data have been recorded by measuring the incoming and the transmitted signals detected by two Ar-filled ionization chambers at ambient pressure. For each position in the oxide and in the metal sides of the metal–oxide interface, good measurement statistics have been achieved by recording a unique extended X-ray absorption fine structure (EXAFS) spectrum in the range of 17 900–18 700 eV. The Athena and Artemis softwares [16] which are part of the Ifeffit program [17] have been used to process and to fit the experimental XAS data. Phase and amplitude have been generated by the FEFF code [18], for the zirconium metal and zirconia [19,20] model compounds.

A similar two-step measurement strategy has been applied at the Nb K-edge to investigate the element-resolved speciation of niobium atoms in the same samples; the measurements have been carried out in fluorescence mode using a Ketek Si detector. To obtain reasonable measurement statistics, five absorption spectra recorded at the Nb K-edge have been merged and then smoothed using 10 iterations. A standard niobium foil has been used to calibrate the experimental data in energy.

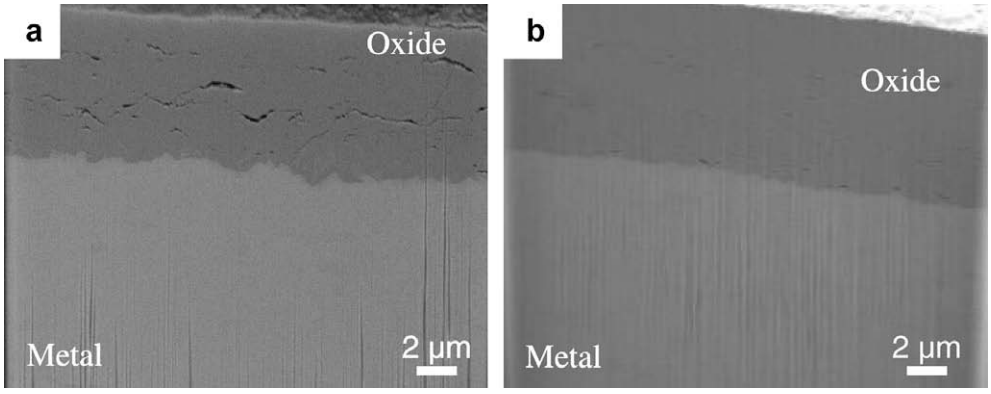

Fig. 1. SEM images which zoom in the metal–oxide interface of (a) the neutron irradiated and (b) the non-irradiated autoclaved reference Zr–2.5%Nb materials (sample preparation: Focused Ion Beam).

3. Results and discussion

The SEM images of the metal–oxide interface recorded on the irradiated and the autoclaved FIB prepared Zr–2.5%Nb materials are presented in Fig. 1. The upper part of each SEM image represents the oxide part of the metal–oxide interface. The two samples exhibit slightly different oxide layer thicknesses: approx. 8 μm in the case of the neutron irradiated and approx. 10 μm for the auto-

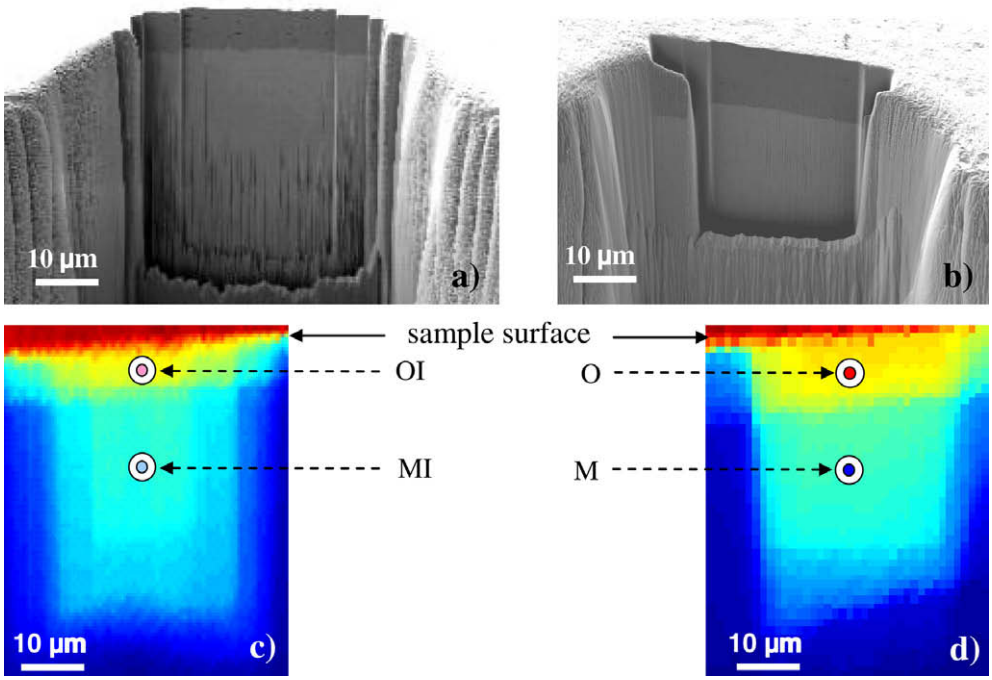

Fig. 2. Electron and X-ray microscopic results for the neutron irradiated (left column) and the non-irradiated autoclaved reference (right column) Zr–2.5%Nb materials: (a, b) SEM images of the sample windows manufactured by FIB, and (c, d) corresponding high resolution 2D STXM images recorded at the Zr K-edge. The positions within the metal (M or MI, I for irradiated) and the oxide (O or OI, I for irradiated) parts of the interface at which micro-XAS investigations are conducted are also shown [acquisition parameters: beam size (horizontal × vertical = approx. 1 μm × 1 μm), detection mode: transmission, room temperature].

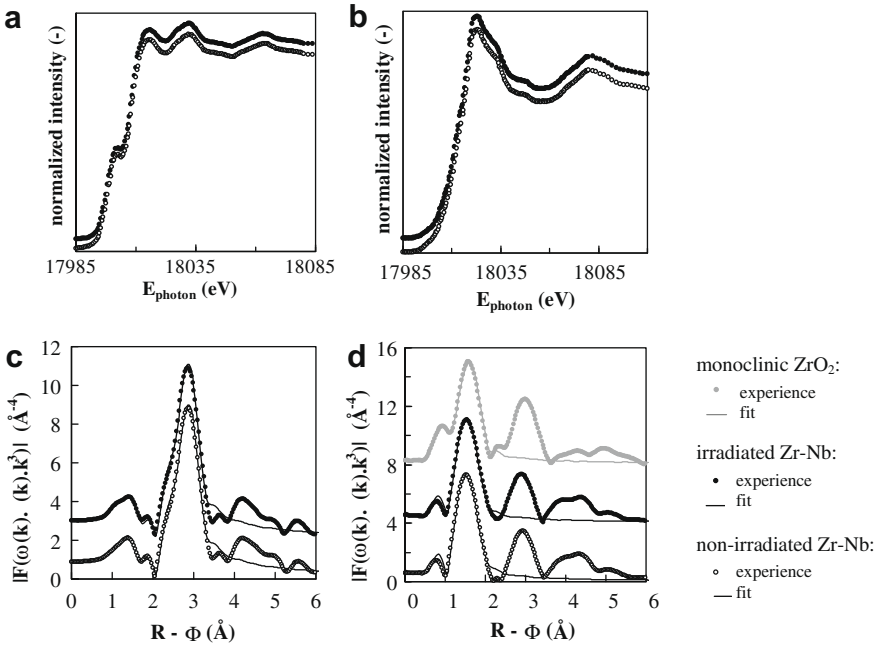

Fig. 3. Comparison of the low energy region of the EXAFS data recorded within the (a) metal and the (b) oxide parts of the metal–oxide interface for the neutron irradiated (black circles) and the non-irradiated autoclaved reference (open black circles) Zr–2.5%Nb materials. The corresponding experimental (symbols) and fit (line) of the Fourier Transforms (FT) of the EXAFS data presented in (a and b) are shown in (c and d), respectively. In (d), the experimental (grey circles) and fit (open grey circles) of the FT of the EXAFS data recorded on monoclinic ZrO_2 are also presented for comparison [acquisition parameters: beam size (horizontal × vertical = approx. 1 μm × 1 μm), detection mode: transmission, room temperature; the absorption spectra and corresponding FT are shifted in *y* direction for better visibility].

claved specimen. By contrast to the autoclaved sample, the irradiated sample shows an undulated metal–oxide interface.

Additional SEM images of the milled windows of the metal–oxide interface have also been recorded for both materials [Fig. 2(a) and (b)]. The images represent the overall view of the window milled down to a thickness of 10 μm. The comparison between these SEM images [Fig. 2(a) and (b)] with the corresponding 2D high resolution zirconium distribution maps of the same regions [Fig. 2(c) and (d)] directly allows the localization of the oxide and the metal parts of the interface. The interface between the metal and the oxide regions is clearly visible. Indeed, the 2D maps at the micrometer scale resolution show a modification in their grey-level contrast, they exhibit dark and bright regions. Just below the sample surface, the bright region represents the oxide layer. While crossing the oxide layer perpendicular to the sample surface, a transition from bright to dark is reached [Fig. 2(c) and (d)]; this transition corresponds to the metal–oxide interface. Underneath this interface, the metal layer with its dark grey-level is visible. This change in the grey-level contrast is due to the difference in density of zirconium (metal part) with respect to zirconia (oxide part).

Knowing the precise location of the metal–oxide interface at a micrometer scale resolution, further spectroscopic investigations of the interface have been achieved by positioning the hard X-ray micro-focused beam at two sample positions (one within the oxide and one within the metal) in order to collect EXAFS data. Fig. 3(a) and (b) shows the effect of neutron irradiation on the low energy region of the Zr K-edge EXAFS spectra recorded in the metal [Fig. 3(a)] and in the oxide [Fig. 3(b)] parts of the interface. It is clear that the spectra recorded in the metal part of the irradiated and the non-irradiated materials are comparable in terms of energy position to that of pure zirconium [13]. By contrast, the absorption spectra recorded within the oxide exhibit very distinct pre-edge and oscillatory structures compared to those recorded within the metal. The concomitance of the pronounced white line of the spectra recorded in the oxide with the energy shift close to 9 eV of the absorption spectra towards higher values [Fig. 3(b)] can be used as a fingerprint of the formal valency of the zirconium absorbing atom. This reveals a zirconium oxide-character whether the sample had been irradiated or not. The oscillatory EXAFS structure of the absorption spectrum also contains useful speciation information of zirconium in the samples. Fig. 3(c) and (d) compare the experimental and the fit of the k^3-weighted Fourier Transforms of the EXAFS data extracted from the absorption spectra presented in Fig. 3(a) and (b), respectively. From the fitting procedure, the averaged local coordination environment of zirconium, i.e. the types of atoms, coordination numbers and distances of the atoms in the surrounding of zirconium can be determined. In the metal part of the interface, the first coordination shell around zirconium thus consists of 12 zirconium atoms at a distance of (3.20 ± 0.03) Å with a Debye–Waller factor equal to $(7.0 \pm 1.5) \times 10^{-3}$ Å^{-2} for the irradiated and the non-irradiated reference samples. The coordination environment for zirconium is similar in the metal part of the interface for the irradiated and the non-irradiated materials, and is comparable to that of hexagonal close-packed zirconium.

In the oxide, the first peak of the Fourier Transform at (2.14 ± 0.03 Å) is related to the oxygen coordination shell. The Debye–Waller factor is not significantly different for the two samples, which means a similar local structural disorder. Concerning the chemical environment of zirconium, a significant fit improvement is obtained when the average coordination number of oxygen atoms is fixed to seven (monoclinic structure) instead of eight (tetragonal structure). By following a complementary fitting approach, i.e. by considering the coordination number of oxygen as a free parameter of the fit, the average coordination number of oxygen atoms is found to be in the range 6.5–7.2 (±10%) for the two samples. All together, this gives a strong hint for a preferential monoclinic structure of zirconium atoms in the oxide, a possible small amount of tetragonal structure being not totally excluded. The coordination environment within 2.5 Å around zirconium atoms is thus almost similar for the irradiated and the non-irradiated reference Zr–2.5%Nb alloys.

The niobium spectroscopic data recorded on the Zr–2.5%Nb materials are presented in Fig. 4. Fig. 4(a) [respectively Fig. 4(b)] compares the Nb K-edge XANES spectra recorded in the metal (resp. in the oxide) parts of the irradiated and the autoclaved reference materials. The absorption spectrum of metallic niobium is added on those figures for comparison. In the metal part, the XANES oscillatory features as well as the absorption threshold energy are similar for the irradiated and autoclaved reference samples revealing a comparable averaged structure and formal valency for niobium. The threshold energy of the Nb K-edge XANES spectra which is similar to that of niobium metal suggests a metallic character of niobium atoms. However, these spectra are not fully identical to that of pure metal niobium, as the (Zr, Nb) phases present in Zr–2.5%Nb alloy are different from a metallic niobium structure [10].

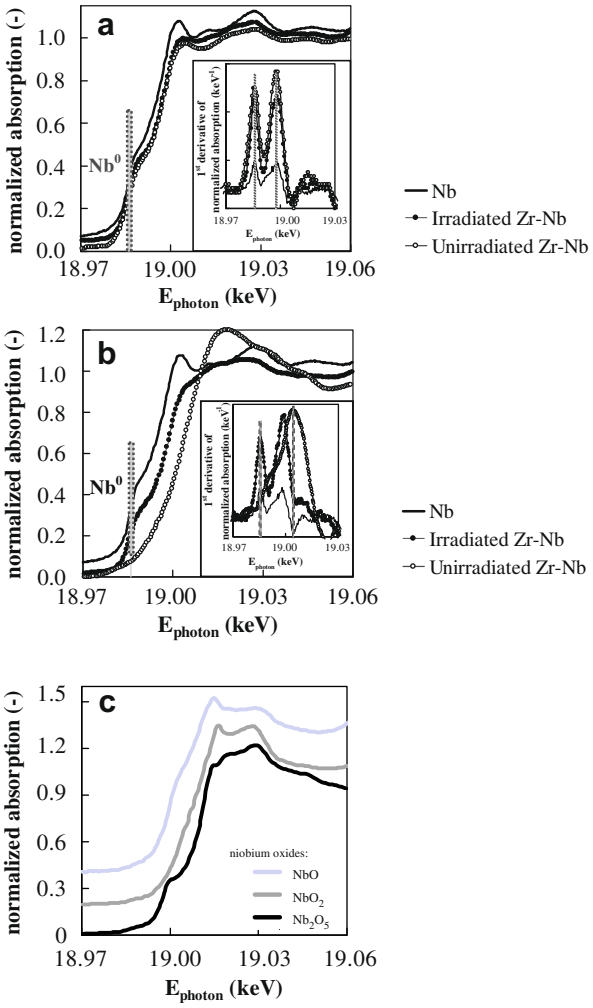

Fig. 4. Nb K-edge XANES spectra recorded in (a) the metal part and (b) the oxide part of the metal–oxide interface for the irradiated (black circles) and the non-irradiated autoclaved reference (open circles) Zr–2.5%Nb materials compared with that of niobium metal sample (black line). (c) Additional XANES spectra recorded on different niobium oxides reference compounds are also reported by way of comparison. The absorption spectra are shifted in *y* direction for better visibility.

In the oxide part, the niobium speciation results which can be extracted from the analysis of the niobium spectroscopic data are as follows. The Nb K-edge XANES spectrum recorded on the irradiated sample is localized at the same threshold energy compared to that of niobium reference sample revealing a metallic nature of the niobium atoms. However, a distinct XANES oscillation structure occurs in this spectrum compared to that of niobium metal. This observation could be explained by the incorporation of oxygen atoms in the Nb-rich phases as observed in previous studies [11,14].

The fact that the absorption spectrum for the non-irradiated autoclaved reference sample has been recorded at a larger distance from the interface with respect to the spectrum recorded on the irradiated sample may explain the observed shift of the threshold energy of the absorption spectrum towards higher energy values. In order to better examine this phenomenon, it is foreseen that the speciation of niobium and zirconium for the Zr–2.5%Nb materials should be studied in a future investigation using the same approach measurement presented in this paper, by recording EXAFS spectra at the Zr and Nb K-edges using micrometer steps along the metal–oxide interface. This will allow to obtain detailed information about the speciation as a function of distance from the interface for both irradiated and non-irradiated materials. It must be noted that PWR environment under H_2 condition is a reducing environment, which could inhibit the oxidation of niobium to a larger distance from the interface, in comparison with the autoclave conditions. The observed shift of threshold energy towards high photon energy could be related to niobium oxide phases formed in the oxide. Indeed, such oxidized niobium phases have already been reported to form in Zr–Nb alloys [10,21]. The comparison of the spectra recorded on the alloys with those obtained on niobium oxides references (NbO, NbO_2 or Nb_2O_5) shows that none of the individual reference spectra fully coincide with that of the alloy. This leads to the conclusion that the averaged niobium local structure in the oxide of the alloy does not correspond to any of the above-mentioned niobium oxide reference phases.

4. Conclusions

Synchrotron-based X-ray microscopic and spectroscopic measurements have been applied to an irradiated and a non-irradiated Zr–2.5%Nb alloys, in view of examination of the speciation of zirconium and niobium in the metal and the oxide layers of the two alloys. Two-dimensional chemical images of the interface with a micrometer resolution have been recorded to localize the metal–oxide interface for both materials. The element-resolved spectroscopic results are as follows. In the metal part of the interface, the coordination environment within 3.5 Å around the zirconium absorbing atom is similar for the irradiated and the non-irradiated materials, and is comparable to that of hexagonal close-packed zirconium. In the oxide part of the interface, no metallic zirconium atoms are present before and after irradiation, and the coordination environment of zirconium in its first coordination shell is not modified by neutron irradiation. In particular, the oxide mainly shows a monoclinic crystal structure both in the non-irradiated and irradiated materials.

In the case of niobium, the atoms present in the metal part of the interface for both the irradiated and the non-irradiated materials exhibit a metallic character, with a different structure with respect to pure niobium metal. The same valency is also found for niobium in the oxide of the irradiated Zr–2.5%Nb alloy, in the vicinity of the metal–oxide interface. In the non-irradiated material, as the Nb K-edge absorption spectrum has been measured at a large distance from the interface, the niobium has an oxide character, and its averaged structure does not correspond to a single NbO, NbO_2 or Nb_2O_5 niobium oxide phase.

Acknowledgments

Acknowledgments are due to S. Cammelli, G. Kuri and C. Proff for their help during the XAS measurements campaign, A. Bullemer for the mounting of the samples onto the special sample holder, and H.-P. Linder for the measurement of the activity of the radioactive materials. The authors wish to thank Kernkraftwerk Gösgen for providing the irradiated sample. Areva is also thanked for providing the autoclaved sample. The SLS proposal review committee is acknowledged for the provision of beamtime. This work was partially founded by swissnuclear.

References

[1] H.G. Kim, Y.H. Jeong, T.H. Kim, J. Nucl. Mater. 326 (2004) 125.
[2] Y.H. Jeong, H.G. Kim, D.J. Kim, B.K. Choi, J.H. Kim, J. Nucl. Mater. 323 (2003) 72.
[3] H. Anada, K. Takeda, S. Hagi, T. Murata, A. Oe, T. Miyashita, Out-of-Pile Corrosion Behaviour and Corrosion Mechanism of NDA for High Burn-up Fuel of PWR, in: Proceeding of the ANS International Topical Meeting on LWR Fuel Performance, IAEA, Park City, 2000, pp. 445–456.
[4] O.S. Ivanov, V.K. Grigorovich, in: Proceeding of the Second United Nations International Conference on the Peaceful Uses of Atomic Energy, Geneva, vol. E-14/P/2046, 1958, pp. 34–51.
[5] R.S. Ambartsumyan, A.A. Kiselev, R.V. Grebennikov, V.A. Myshkin, L.J. Tsuprun, A.F. Nikulina, in: Proceeding of the Second United Nations International Conference on the Peaceful Uses of Atomic Energy, Geneva, vol. E-14/P/2044, 1958, pp. 12–33.
[6] A. Yilmazbayhan, A.T. Motta, R.J. Comstock, G.P. Sabol, B. Lai, Z. Cai, J. Nucl. Mater. 324 (2004) 6.
[7] J.L. Béchade, R. Dralet, P. Goudeau, P. Yvon, Mater. Sci. Forum 347–349 (2000) 471.
[8] N. Pétigny, P. Barberis, C. Lemaignan, Ch. Valot, M. Lallemant, J. Nucl. Mater. 280 (2000) 318.
[9] D. Pêcheur, J. Nucl. Mater. 278 (2000) 195.
[10] Y.P. Lin, O.T. Woo, J. Nucl. Mater. 277 (2000) 11.
[11] S. Abolhassani, R. Restani, T. Rebac, F. Groeschel, W. Hoffelner, G. Bart, W. Goll, F. Aeschbach, J. ASTM Int. 2 (2005) 1.
[12] A. Froideval, C. Degueldre, C.U. Segre, M.A. Pouchon, D. Grolimund, Corros. Sci. 50 (2008) 1313.
[13] C. Degueldre, K. Dardenne, Nucl. Instrum. and Meth. B 238 (2005) 323.
[14] P. Bossis, J. Thomazet, F. Lefebvre, in: Zirconium in the Nuclear Industry: Thirteenth International Symposium, 2002, pp. 190–217.
[15] D. Grolimund, A.M. Scheidegger, J.F. van der Veen, R. Abela, Layout of the microXAS beamline at SLS, PSI Scientific Report, vol. IV, 2002, ISSN 1423–7334, pp. 139–148.
[16] B. Ravel, M. Newville, J. Synchrotron Rad. 12 (2005) 537.
[17] M. Newville, J. Synchrotron Rad. 8 (2001) 322.
[18] A.L. Ankudinov, B. Ravel, J.J. Rehr, S.D. Conradson, Phys. Rev. B 58 (1998) 7565.
[19] D.K. Smith, H.W. Newkirk, Acta Crystallogr. 18 (1965) 983.
[20] J.D. McCullough, K.N. Trueblood, Acta Crystallogr. 12 (1959) 507.
[21] D. Khatamian, S.D. Lalonde, J. Nucl. Mater. 245 (1997) 10.